Eur Biophys J (2011) 40:437–446
DOI 10.1007/s00249-010-0652-5

ORIGINAL PAPER

# QCM-D fingerprinting of membrane-active peptides

**George A. McCubbin · Slavica Praporski · Stefania Piantavigna · Daniel Knappe · Ralf Hoffmann · John H. Bowie · Frances Separovic · Lisandra L. Martin**

Received: 11 October 2010 / Revised: 17 November 2010 / Accepted: 23 November 2010 / Published online: 16 December 2010


**Abstract** The increasing prevalence of antibiotic-resistant bacteria is becoming a public health crisis. Antimicrobial peptides (AMPs) are a promising solution, because bacterial resistance is less likely. Quartz crystal microbalance with dissipation monitoring (QCM-D) is a versatile and valuable technique for investigation of these peptides. This article looks at the different approaches to the interpretation of QCM-D data, showing how to extract the maximum information from the data. Five AMPs of diverse charge, length and activity are used as case studies: caerin 1.1 wild-type, two caerin 1.1 mutants (Gly15Gly19-caerin 1.1 and Ala15Ala19-caerin 1.1), aurein 1.2 and oncocin. The interaction between the AMP and a 1,2-dimyristoyl-*sn*-glycero-3-phosphocholine (DMPC) membrane is analysed *inter alia* using frequency–dissipation plots ($\Delta f$–$\Delta D$ plots) to ascertain the mechanism of action of the AMP. The $\Delta f$–$\Delta D$ plot can then be used to provide a fingerprint for the AMP–membrane interaction. Building up a database of these fingerprints for all known AMPs will enable the relationship between AMP structure and membrane activity to be better understood, hopefully leading to the future development of antibiotics without bacterial resistance.

**Keywords** Antimicrobial peptide · Quartz crystal microbalance · Frequency–dissipation plot · Membrane pore · Membrane disruption

**Abbreviations**

| | |
|---|---|
| AMP | Antimicrobial peptide |
| QCM-D | Quartz crystal microbalance with dissipation monitoring |
| DMPC | 1,2-Dimyristoyl-*sn*-glycero-3-phosphocholine |
| MPA | 3-Mercaptopropionic acid |
| DMPG | 1,2-Dimyristoyl-*sn*-glycero-3-phospho-*rac*-(1-glycerol) |
| PBS | Phosphate buffered saline |
| AFM | Atomic force microscopy |

## Introduction

There is an urgent need for novel antibacterial drugs. The Infectious Diseases Society of America estimates that 70% of bacterial infections acquired in hospitals are resistant to at least one antibiotic and, in 2002, there were 362,000 estimated cases of antibiotic-resistant infections in US hospitals (IDSA 2004). Despite the increasing need, the development of new antibiotics is dwindling. In 2006, only six antibiotics were in phase 2 or phase 3 clinical trials,

Membrane-active peptides: 455th WE-Heraeus-Seminar and AMP 2010 Workshop.

G. A. McCubbin · S. Praporski · S. Piantavigna · L. L. Martin (✉)
School of Chemistry, Monash University, Clayton, VIC 3800, Australia
e-mail: Lisa.Martin@monash.edu

D. Knappe · R. Hoffmann
Institute of Bioanalytical Chemistry, Leipzig University, 04103 Leipzig, Germany

J. H. Bowie
Department of Chemistry, The University of Adelaide, Adelaide, SA 5005, Australia

F. Separovic
School of Chemistry, Bio21 Institute, University of Melbourne, Melbourne, VIC 3010, Australia

compared with 313 other drugs (Katz et al. 2006). Antimicrobial peptides (AMPs) are promising candidates for the next generation of antibiotics. Generally, they are selective, act rapidly and have broad-spectrum activity (Gordon et al. 2005; Shai 2002). Importantly, bacterial resistance to AMPs is considered "improbable" (Zasloff 2002). The retention of their antimicrobial activity for millions of years demonstrates such improbability.

Most known AMPs are linear, short (<100 amino acids), cationic, composed of predominantly hydrophobic residues (≥50%) and unstructured in water, and form amphipathic α-helical structures in a membrane environment (Powers and Hancock 2003). AMPs kill bacteria via a diverse range of mechanisms; for example, they can interact with the lipid membrane via a 'pore' or 'carpet' mechanism (Shai 1999). According to the 'pore' mechanism, the peptides span the bilayer perpendicular to the membrane surface and assemble to form a pore lined by peptides (called 'barrel-stave') or peptides and lipid ('toroidal'). Conversely, in the 'carpet' mechanism, the peptides sit on the bilayer parallel to the surface with their hydrophobic face embedded into the hydrophobic core of the membrane. Once a threshold concentration is reached, the peptides disrupt the bilayer in a detergent-like manner. Both mechanisms kill the cell by allowing free diffusion of species into and out of the cell, either by permeabilising the bilayer or simply destroying it. AMPs can also act on intracellular targets, leaving the lipid membrane intact (Shai 2002). Often, AMPs will adopt more than one of these mechanisms, explaining why the development of bacterial resistance towards them is so difficult (Peschel and Sahl 2006).

Three fundamental questions are raised when investigating an AMP: Is it selective for bacteria? Does it have high activity towards bacteria? And, how does it interact with the membrane? A wide range of biophysical techniques have been employed to help answer these questions; for example, solid-state nuclear magnetic resonance (NMR) (Balla et al. 2004; Marcotte et al. 2003), fluorescence spectroscopy (Ambroggio et al. 2005), atomic force microscopy (Lam et al. 2006; Mechler et al. 2007) and surface plasmon resonance (Papo and Shai 2003). Quartz crystal microbalance with dissipation monitoring (QCM-D) has been the subject of a small number of studies investigating AMPs (Briand et al. 2010; Christ et al. 2007; Knappe et al. 2010; Mechler et al. 2007; Nielsen and Otzen 2010; Piantavigna et al. 2009; Sherman et al. 2009). QCM-D is an attractive technique because it examines the interaction between an AMP and a biological membrane in real time and in situ, and provides information about the mass and structural changes occurring to the membrane (Mechler et al. 2007). Therefore, using this single instrument, it is possible to answer all three questions posed above. This study will demonstrate different methods of presenting the raw data obtained by QCM-D and how these plots can be interpreted to yield the maximum information about AMPs.

## Principles of QCM-D

In a QCM instrument, an alternating-current (AC) voltage is applied across a gold-coated quartz chip to cause the chip to oscillate in shear mode at its fundamental resonance frequency and harmonics of the fundamental frequency. This frequency of oscillation is denoted by $f_n$, where $n$ is the harmonic number. When mass is adsorbed to the gold surface, the resonance frequency *decreases* proportional to the added mass (Sauerbrey 1959). In addition, in a QCM-D instrument, the driving AC voltage is periodically removed (about once per second) to measure the energy loss of the chip into the surrounding environment. The dissipation factor ($D$) is calculated from this energy loss according to the equation (Rodahl et al. 1995)

$$D = \frac{E_{\text{dissipated}}}{2\pi E_{\text{stored}}}, \quad (1)$$

where $E_{\text{dissipated}}$ is the energy lost during a single oscillation after removing the driving voltage and $E_{\text{stored}}$ is the initial energy of the chip. A high $D$ means the chip loses its energy quickly and suggests there is something thick, soft or loose on the surface; conversely, a low $D$ suggests the film on the surface is rigid and compact (Rodahl et al. 1997).

Thus, changes in $f$ and $D$ give information about mass and structure, respectively. In addition, the $f$ and $D$ values for the different harmonics can provide three-dimensional information (Mechler et al. 2007). The penetration depth of the harmonic wave is inversely proportional to the frequency of the wave (Rodahl and Kasemo 1996). Therefore, higher harmonics probe close to the surface of the quartz chip, while lower harmonics probe further away from the surface. The following case studies use the third, fifth, seventh and ninth harmonics. The fundamental frequency is not used as, sensing the furthest from the chip surface, it is very sensitive to flow changes within the cell and thus gives noisy and unreliable data.

When referring to the 'mass' detected by the QCM-D, it is important to remember that it includes both the dry mass of the materials on the chip and associated water that is coupled to the chip due to direct hydration of the materials, entrapment in cavities in the film or viscous drag (Höök and Kasemo 2001). This has two notable consequences: firstly, the mass determined by the QCM-D may be significantly larger than the dry mass [even as much as four times larger, depending on the system (Rickert et al. 1997)]; and, secondly, it will cause an inherent differential response in the harmonics for thick films, as the third

harmonic will probe both the film on the chip and the bulk solution that is coupled to the chip whereas the ninth harmonic will only probe the film.

In a typical experiment, a 1,2-dimyristoyl-*sn*-glycero-3-phosphocholine (DMPC) 'bilayer' is deposited on the gold surface modified with 3-mercaptopropionic acid (MPA), to mimic the cell membrane of eukaryotes. Other cell membranes can be mimicked by using different lipid compositions; for example, DMPC/1,2-dimyristoyl-*sn*-glycero-3-phospho-*rac*-(1-glycerol) (DMPG) mimics prokaryotic cell membranes (Mechler et al. 2007). Bilayer deposition is achieved by flowing a solution of the liposomes through the QCM-D cell. The liposomes adsorb and spontaneously rupture on the MPA surface, forming a lipid bilayer (Mechler et al. 2009). It is hypothesised that a decrease in resonance frequency of ca. 15 Hz at the seventh harmonic corresponds to one complete lipid bilayer (Mechler et al. 2009), so flow is stopped when this value is reached. After equilibration with phosphate buffered saline (PBS), the peptide solution is then introduced into the cell. The peptide is left to incubate with the lipid bilayer before being rinsed with PBS. In all experiments in this paper, the time window presented begins when the peptide was introduced into the cell and ends immediately before the PBS rinse (except for Fig. 6, where the PBS rinse is shown).

## $\Delta f$–$\Delta D$ plot interpretation

Once the QCM-D experiment has been completed, we commonly use three methods to present and interpret the data collected. Firstly, $\Delta f$–$t$ and $\Delta D$–$t$ plots are prepared, usually showing one concentration with all harmonics (e.g. Figs. 3a or 4a). The $\Delta f$ and $\Delta D$ parameters refer to the raw $f$ and $D$ data at a certain time, normalised by the values at the start of the experiment (i.e. $\Delta f_{\text{at time}=t} = f_{\text{at time}=t} - f_{\text{at time}=0}$). Secondly, the raw data may be analysed in the commercial software package QTools (Q-Sense AB, Västra Frölunda, Sweden) to extract either the Sauerbrey mass of the film, or its thickness and viscoelasticity by using the Voigt viscoelastic model (Voinova et al. 1999). Finally, plots of $\Delta f$ versus $\Delta D$ may be prepared (hereinafter called '$\Delta f$–$\Delta D$ plots').

$\Delta f$–$\Delta D$ plots are a unique way of presenting the effect of a peptide on a lipid bilayer, first introduced by Rodahl et al. (1997). They essentially show how the structure of the lipid bilayer changes per unit mass addition. $\Delta f$–$\Delta D$ plots consist of a number of discrete points. Each point represents the value of $\Delta f$ and $\Delta D$ at a particular point in time. $\Delta f$ values are plotted in *reverse* on the $x$-axis ($+ \rightarrow -$) in order to reflect mass increase (i.e. $-\Delta f \cong \Delta m$), and $\Delta D$ values are plotted on the $y$-axis (Fig. 1). Thus the point ($x$, $y$) corresponds to ($\Delta f_{\text{time}=t}$, $\Delta D_{\text{time}=t}$). In $\Delta f$–$\Delta D$ plots, time is *not* an explicit parameter. However, time can be inferred. The

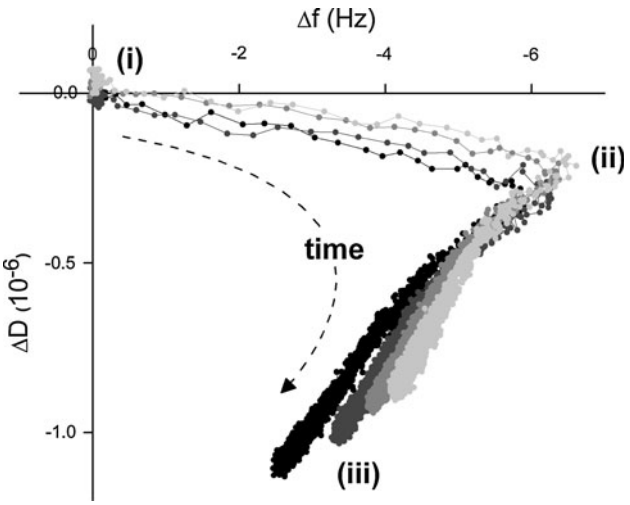


**Fig. 1** Example of a $\Delta f$–$\Delta D$ plot for the addition of a peptide solution to a lipid bilayer. The behaviour of the third, fifth, seventh and ninth harmonics are shown (*darkest* to *lightest* dots). Connecting lines are used as a visual aid only. All figures in this paper were prepared using OriginPro 8 (OriginLab Corp., Northampton, USA)

point (0,0) corresponds to time = 0 min, and time increases following the trace outward from the origin (Fig. 1).

$\Delta f$–$\Delta D$ plots are useful for a number of reasons. Firstly, they quickly show the behaviour of the peptide. This will be explained below. Secondly, they highlight mechanistic processes. Generally, where there is a change in the direction of the trace this suggests a different process is occurring [e.g. (i)–(ii) and (ii)–(iii) in Fig. 1] (Rodahl et al. 1997). Thirdly, kinetic information can be extracted from the plots. Data points are acquired by the QCM-D every ca. 1 s, thus where the points are spread out the process is rapid [e.g. (i)–(ii) in Fig. 1], and where the points are closely spaced the process is slow [e.g. (ii)–(iii) in Fig. 1] (Rodahl et al. 1997). Finally, the trace can be used as a *fingerprint* for the interaction between that peptide with the membrane. This may enable relationships between peptides to be discovered. Peptides with similar $\Delta f$–$\Delta D$ traces have similar mechanisms of action, which may help us understand which amino acid residues are responsible for that mechanism and, hence, activity.

To interpret the behaviour of the peptide during each process, it is useful to draw an arrow beginning at the start of the process and pointing towards the end of that process (e.g. for the first process in Fig. 1, the arrow would be pointing south-east). Next, use Fig. 2 as a guide to ascertain what that arrow indicates. If the arrow is pointing south, the process is causing the bilayer to become more rigid; conversely, if the arrow is pointing north, the bilayer is becoming less rigid. If the arrow is pointing east, the process adds mass to the bilayer; conversely, if the arrow is pointing west, there is mass loss from the bilayer. For example, a south-east arrow suggests an increase in mass

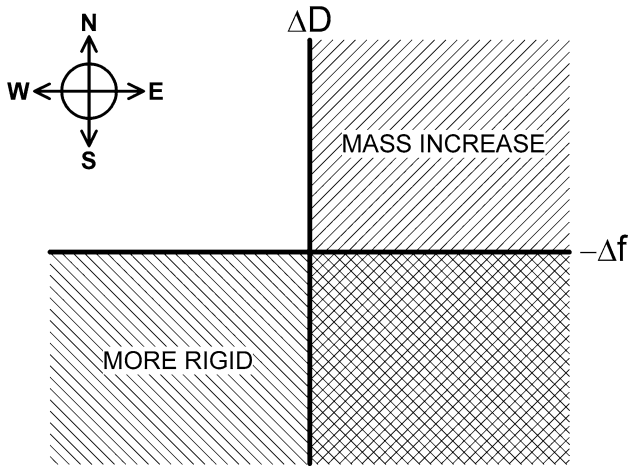


**Fig. 2** Interpretative guide for $\Delta f$–$\Delta D$ plots. North is up, and east is to the right. See text for explanation

with a corresponding increase in rigidity. This paper provides four case studies to assist in the understanding of this interpretation process.

## Peptides under investigation

Five diverse AMPs will be used as case studies in this paper: caerin 1.1 wild-type, Gly15Gly19-caerin 1.1, Ala15Ala19-caerin 1.1, aurein 1.2 and oncocin. The amino acid sequences of these peptides are provided in Table 1.

Caerin 1.1 is a wide-spectrum antibiotic from the Australian green tree frog, *Litoria splendida*. It has higher activity against Gram-positive than Gram-negative bacteria (Wong et al. 1997) and also has antiviral and anticancer properties (VanCompernolle et al. 2005). The solution-state structure of caerin 1.1 shows that it forms two amphipathic α-helices (between Leu2-Lys11 and Val17-His24) with a central flexible region containing two proline residues (at positions 15 and 19), which cause the C- and N-terminal helices to be angled at 105° with respect to each other, such that it resembles a boomerang (Pukala et al. 2004; Wong et al. 1997).

In Gly15Gly19-caerin 1.1 and Ala15Ala19-caerin 1.1, the two proline residues have been replaced with two glycines and two alanines, respectively. The substitution increases the angle between the two α-helices, making the peptides more linear, and decreases their flexibility (Pukala et al. 2004). This results in decreased antibiotic activity, with the glycine mutant having only intermediate activity and the alanine mutant being essentially inactive (Pukala et al. 2004). It is suggested that the kink in the structure of caerin 1.1 wild-type reorientates the two α-helices such that there is a continuous hydrophobic and hydrophilic face; however, as a result of the substitutions, the kink is significantly reduced in the mutants, causing Lys11 to lie at the interface of the two faces in Gly15Gly19-caerin 1.1 and actually project into the hydrophobic face in Ala15Ala19-caerin 1.1 (Pukala et al. 2004).

Aurein 1.2 is a short AMP secreted by the southern bell frog, *Litoria raniformis*. It shows both antibiotic and anticancer activity (Rozek et al. 2000). The solution structure of aurein 1.2 shows it forms an α-helix with well-defined hydrophilic and hydrophobic zones (Rozek et al. 2000). It was hypothesised by Rozek et al. (2000) that aurein 1.2 is unable to span the lipid bilayer because, with 13 amino acid residues, it is too short, and thus operates via the carpet mechanism. This was confirmed by QCM-D results published by our group (Mechler et al. 2007).

Finally, oncocin (peptide 10) is a novel AMP based on the native *Oncopeltus* antibacterial peptide isolated from *Oncopeltus fasciatus* (Knappe et al. 2010). Oncocin was optimised to have high activity against Gram-negative bacteria, low toxicity towards human cell lines and human red blood cells and a prolonged biological half-life. Unlike the other AMPs discussed in this article, oncocin exerts its antibacterial activity through a non-lytic, bacteriostatic mechanism. It was demonstrated by Knappe et al. (2010) that oncocin freely penetrates bacterial membranes, as evidenced by confocal fluorescence microscopy and QCM-D.

This research article will analyse the QCM-D data obtained for the interaction of these five AMPs with mammalian-like DMPC membranes, showing how $\Delta f$–$\Delta D$ plots aid in the interpretation of their mode of action. The first two case studies for caerin 1.1 wild-type and Gly15Gly19-caerin 1.1/Ala15Ala19-caerin 1.1 illustrate how $\Delta f$–$\Delta D$ plots may be used to determine the individual mechanistic processes that occur during the interaction

**Table 1** Sequence of AMPs investigated

| Name | Sequence | Ref. |
|---|---|---|
| Caerin 1.1 wild-type | GLLSVLGSVAKHVLPHVVPVIAEHL-$NH_2$ | (Stone et al. 1992) |
| Gly15Gly19-caerin 1.1 | GLLSVLGSVAKHVLGHVVGVIAEHL-$NH_2$ | (Pukala et al. 2004) |
| Ala15Ala19-caerin 1.1 | GLLSVLGSVAKHVLAHVVAVIAEHL-$NH_2$ | (Pukala et al. 2004) |
| Aurein 1.2 | GLFDIIKKIAESF-$NH_2$ | (Rozek et al. 2000) |
| Oncocin (peptide 10) | VDKPPYLPRPRPPRRIYNR-$NH_2$ | (Knappe et al. 2010) |

between peptide with the membrane. The last two case studies for aurein 1.2 and oncocin show two different ways $\Delta f$–$\Delta D$ plots can be used to extract additional information, that is, by comparing them for different concentrations or by including the buffer rinse that is performed after peptide incubation.

## Case studies

### Case study 1: caerin 1.1 wild-type

All experiments in this study were conducted as previously reported by Mechler et al. (2007). Figure 3a shows the simplest representation of QCM-D data. The top panel in Fig. 3a is a $\Delta f$–$t$ plot, which shows the changes in mass of the membrane after the introduction of the peptide solution. The bottom panel (Fig. 3a) is a $\Delta D$–$t$ plot, which shows changes in the structure of the membrane. It can be concluded from these plots that, upon interaction of caerin 1.1 wild-type with a DMPC membrane, there is an overall loss of mass from and a stiffening of the membrane, evidenced by a positive shift in the $\Delta f$ values at the end of the experiment with respect to the start and a negative shift in the $\Delta D$ values.

The $\Delta f$–$\Delta D$ plot is a complementary method of presenting the data (Fig. 3b). One advantage of the $\Delta f$–$\Delta D$ plot is that it highlights the mechanistic processes occurring during the experiment (Rodahl et al. 1997); for example, in Fig. 3b there are two distinct turning points in the trace, which suggests that there are three mechanistic processes [labelled (i)–(iii) in Fig. 3b].

The first process can be represented by a north-east arrow [arrow (i) in Fig. 3b], which, according to Fig. 2, is interpreted as an increase in mass of the membrane with a corresponding loss of rigidity. In the experiment shown, this process was very rapid (taking 40 s). However, in some experiments it is not observed at all, suggesting that it is a real effect, albeit dependent on variables such as membrane structure, rather than an apparent effect caused by a difference in density or viscosity of the peptide solution being introduced in the QCM-D chamber (Kanazawa and Gordon 1985). This process corresponds to the addition of peptide to the membrane, until a critical concentration is reached.

During the second process, represented by a south-west arrow [arrow (ii) in Fig. 3b], mass is rapidly lost from the membrane and it becomes more rigid. This suggests that caerin 1.1 wild-type *disrupts* mammalian-like DMPC membranes. In Fig. 3b the traces of the four harmonics do not overlap, but rather they are spread out. The third and fifth harmonics, which probe further from the chip surface, show the greatest loss of mass, suggesting that more mass is lost from the top of the membrane (Mechler et al. 2007). Rapid disruption was observed at peptide concentrations of $\geq$5 μM, with a slow gradual disruption at 2 μM, showing the potency of this peptide towards DMPC membranes (data not shown). Its potency is also emphasised by the speed of membrane disruption, with both processes 1 and 2 taking less than 2 min.

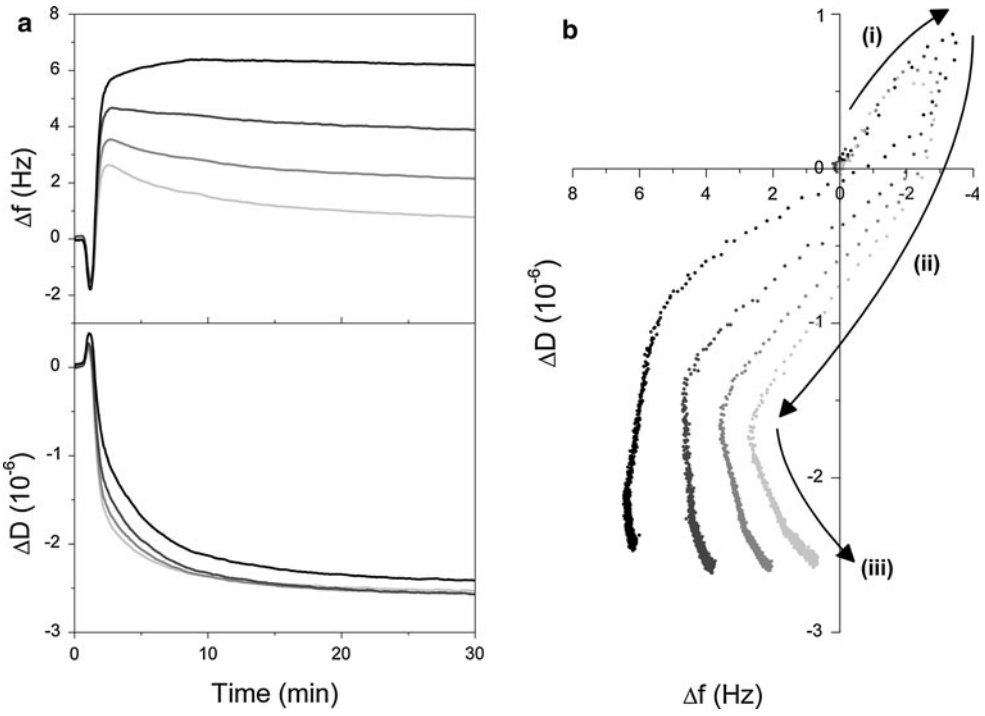


**Fig. 3** Interaction of caerin 1.1 wild-type with DMPC membrane. **a** Change in $\Delta f$ and $\Delta D$ with time on introduction of a 20 μM solution of the peptide into the QCM-D chamber. The response of the third, fifth, seventh and ninth harmonics are shown (*darkest* to *lightest* lines). $\Delta f$-time and $\Delta D$-time plots have been smoothed using the Adjacent-Averaging method, with 20 points of window. **b** Corresponding $\Delta f$–$\Delta D$ plot for the 20 μM sample. To assist with interpretation, *arrows* representing each distinct mechanistic process are shown. The *arrows* labelled (i)–(iii) correspond to the first to third processes, respectively

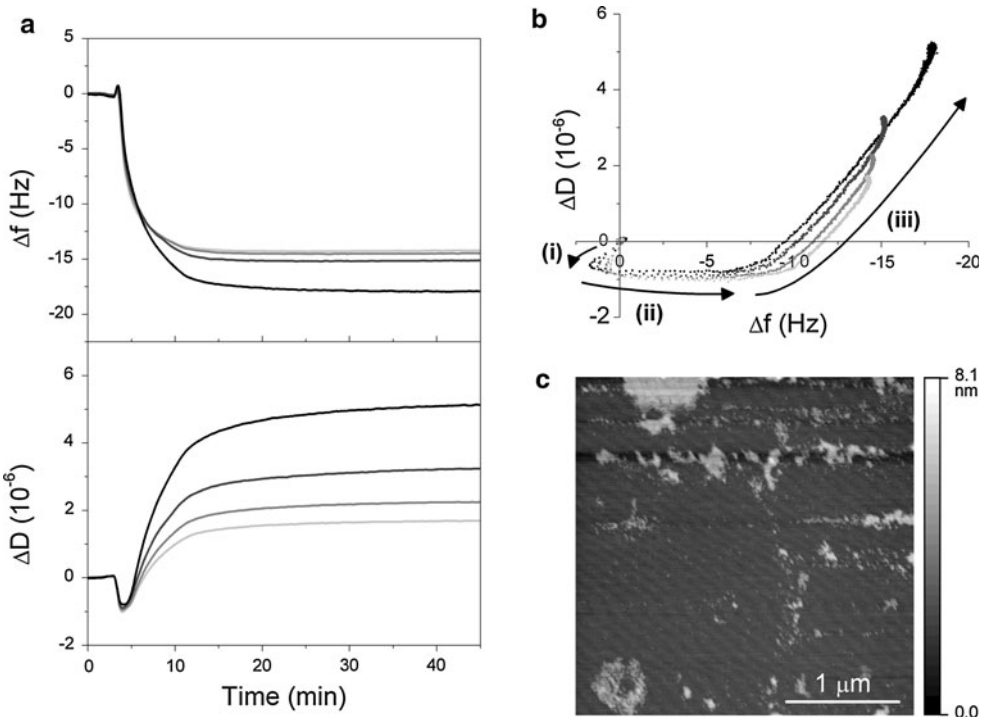


**Fig. 4** Interaction of caerin 1.1 mutants with DMPC membrane. **a** Change in $\Delta f$ and $\Delta D$ with time on introduction of a 20 μM solution of Gly15Gly19-caerin 1.1 into the QCM-D chamber. The response of the third, fifth, seventh and ninth harmonics are shown (*darkest* to *lightest* lines). $\Delta f$-time and $\Delta D$-time plots have been smoothed using the Adjacent-Averaging method, with 20 points of window. **b** Corresponding $\Delta f$–$\Delta D$ plot for the 20 μM sample. To assist with interpretation, *arrows* representing each distinct mechanistic process are shown. The *arrows* labelled (i)–(iii) correspond to the first to third processes, respectively. **c** AFM image of 0.5 μg Ala15Ala19-caerin 1.1 incubated with a DMPC membrane in PBS. Image was processed using the free software Gwyddion 2.20

Finally, the third process [arrow (iii) in Fig. 3b] involves very slow mass gain on the higher harmonics with a continuing increase in rigidity of the membrane. This process is consistent with a rearrangement of the peptide and lipid remaining on the chip. During this process there is no overall change in mass of the film, evidenced by there being no change in the third harmonic, but mass gain in the chip surface-sensing higher harmonics. This suggests that weakly bound material is diffusing from the top of the film inwards, thus resulting in a more densely packed film with no overall change in mass.

In summary, caerin 1.1 wild-type disrupts DMPC membranes. The three distinct processes in this mechanism (addition, disruption and rearrangement), while not readily identifiable from the $\Delta f$–$t$ and $\Delta D$–$t$ plots, are clearly distinguished in the $\Delta f$–$\Delta D$ plot. By including all harmonics in the $\Delta f$–$\Delta D$ plot, it is possible to obtain information about the three-dimensional structure of the lipid membrane. This conclusion is consistent with solid-state NMR studies, which have shown that caerin 1.1 wild-type appears to "partially insert" before "cell lysis" in DMPC bilayers (Marcotte et al. 2003). However, we can now define this peptide as acting on DMPC by a disruption consistent with a *carpet mechanism*. This conclusion differs from our earlier QCM-D work that suggested that caerin 1.1 wild-type formed transmembrane pores (Mechler et al. 2007). One possible explanation for this discrepancy is the presence of trace amounts of trifluoroacetic acid in the original peptide sample, which were not present in the sample used in this study.

## Case study 2: Gly15Gly19-caerin 1.1 and Ala15Ala19-caerin 1.1

Fig. 4a shows the $\Delta f$–$t$ and $\Delta D$–$t$ plots for Gly15Gly19-caerin 1.1. Remarkably, when comparing the plots in Figs. 3a and 4a, it is observed that the $\Delta f$–$t$ plot in Fig. 4a resembles the $\Delta D$–$t$ plot in Fig. 3a. Thus, substitution of the two proline residues in the wild-type with two glycines radically changes the behaviour of the peptide. The only similarity between the interaction of the wild-type and the mutant peptide with a DMPC membrane is that their $\Delta f$–$\Delta D$ plots both indicate a three-stage mechanism (Fig. 4b). The behaviour of Ala15Ala19-caerin 1.1 is very similar to that of Gly15Gly19-caerin 1.1, showing the same $\Delta f$–$\Delta D$ fingerprint with only slight differences in magnitude, hence the QCM-D data is not presented.

In interpreting the $\Delta f$–$\Delta D$ plot (Fig. 4b) it is useful to work in reverse, that is, first to understand the overall effect of the peptide on the membrane, and then to elucidate how this outcome is reached. Therefore, starting with the third process [arrow (iii) in Fig. 4b], we note there is an increase in both mass and energy dissipation. This process corresponds to *aggregation* of the peptide on the surface. Figure 4b illustrates this aggregation, as the mass and dissipation increase is greatest for the third harmonic, suggesting that there is a non-rigid structure extending high above the chip surface. Furthermore, this conclusion is supported by atomic force microscopy (AFM) images, which reveal that Ala15Ala19-caerin 1.1 forms large aggregates, some as large as 800 nm in width and 8 nm in

height, on DMPC bilayers (Fig. 4c). Clearly, the substitutions have changed the disruptive mechanism of the wild-type peptide to a non-disruptive mechanism on DMPC membranes. Accordingly, Gly15Gly19-caerin 1.1 is a better candidate for an antibiotic because it does not disrupt mammalian membranes, while having the same activity against certain bacteria as the wild-type, including *Bacillus cereus*, *Micrococcus luteus* and *Streptococcus uberis* (Pukala et al. 2004).

To ascertain whether the membrane was causing or promoting aggregation, Ala15Ala19-caerin 1.1 was added to an MPA-modified chip without lipid. A similar amount of peptide added to the surface, but it formed a very compact structure, as evidenced by a change in $\Delta D$ of $<0.5 \times 10^{-6}$ and no spreading of the harmonics (data not shown). Thus, while the membrane is not causing aggregation, it does facilitate the formation of larger and highly dissipating aggregates.

In the second process [arrow (ii) in Fig. 4b], mass rapidly increases with no change in energy dissipation. It is not uncommon for peptides to bind to bilayers with no change in dissipation; we have observed this for non-lytic AMPs, e.g. apidaecin 1a and 1b (Piantavigna et al. 2009) and oncocin (Knappe et al. 2010). The rationale behind this is that non-lytic AMPs must be able to freely traverse the membrane, which requires a low energy for membrane penetration and thus suggests that changes to the membrane during penetration must be minimised. Thus, during this second process, peptide is added to the membrane with little conformation change. Once saturation of the membrane is achieved, the third process commences.

The first process can be represented by a south-west arrow [arrow (i) in Fig. 4b], which suggests a loss of mass from the chip surface with a corresponding decrease in energy dissipation (Fig. 2). This process was observed at all peptide concentrations and in all experiments involving Gly15Gly19-caerin 1.1. A similar amount of mass is lost at all concentrations; however, the mass loss is slower for the lower concentrations (data not shown). Furthermore, this process was only observed on interaction with DMPC membranes and not DMPC/DMPG membranes (data not shown). This suggests that, similar to the first process for caerin 1.1 wild-type, this process cannot be attributed to the difference in density or viscosity of the peptide solution, otherwise it would be observed in all experiments regardless of lipid composition and at different magnitudes for the different peptide concentrations. Clearly, the introduction of the peptide solution causes an instantaneous structural change to the membrane. This structural change may expel water molecules associated to the lipid headgroups, offsetting any increase in mass due to peptide addition (Nilebäck et al. 2010). However, the actual mechanism through which this is achieved is, at the moment, unclear.

The $\Delta f$–$\Delta D$ plot again allows us to access mechanistic information not readily apparent from the individual $\Delta f$–$t$ and $\Delta D$–$t$ plots. For the addition of Gly15Gly19-caerin 1.1 and Ala15Ala19-caerin 1.1 to a DMPC membrane, three processes are observed. These are consistent with, firstly, addition of a small amount of peptide to the membrane in a manner that changes its structure, secondly, addition of peptide until membrane saturation and, thirdly, further addition of peptide to the surface of the membrane to form aggregates.

## Case study 3: aurein 1.2

In the previous case studies, the response of the different harmonics was used to ascertain the mechanism of action of the peptides. An important additional source of information is the behaviour of the peptide over a range of concentrations. In general, the higher concentrations reveal the overall mode of action of the peptide (e.g. membrane disruption, pore formation), while the lower concentrations elucidate how this mode of action is achieved (e.g. the orientation of the peptide in the membrane, the effect of binding on the structure of the membrane) (Mechler et al. 2007). The aurein 1.2 case study provides an illustration of this strategy. $\Delta f$–$t$ plots of a low concentration of aurein 1.2 (5 μM) and a higher concentration (10 μM) are shown in Fig. 5a and c, respectively. The corresponding $\Delta f$–$\Delta D$ plots are shown in Fig. 5b and d.

Beginning with the high-concentration sample (Fig. 5c and d), it is observed that there is essentially one mechanistic process that can be represented by a south-west arrow, which indicates a rapid loss of mass with a decrease in energy dissipation (Fig. 2). Thus, aurein 1.2 causes an *instantaneous disruption* of the DMPC membrane. Similar to caerin 1.1 wild-type, the spreading of the harmonics suggests that more mass is lost from the surface of the membrane. However, because of the rate of this process, it is difficult to identify how this disruption proceeds. This is where the data from the lower peptide concentration becomes useful.

The low-concentration sample (Fig. 5a and b) causes a decrease in resonance frequency at the seventh and ninth harmonics, but an increase in frequency at the third and fifth harmonics; that is, the harmonics sensing closer to the chip surface (seventh and ninth) show a mass gain, but those sensing further away from the surface (third and fifth) show a mass loss. This could correspond to an addition of peptide to the membrane, followed by an instantaneous redistribution of mass from the top leaflet to the bottom leaflet. However, the third harmonic essentially represents what is happening to the overall mass of the membrane on the surface. A redistribution of mass would not cause a mass loss at the third harmonic, as mass is conserved.

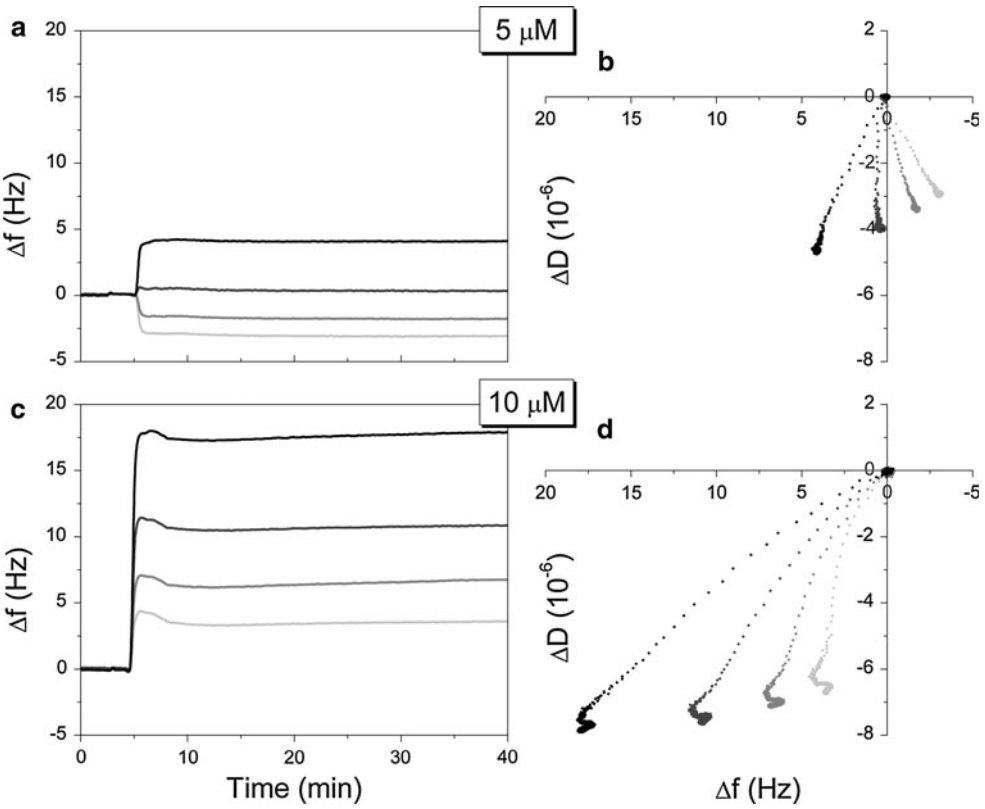


**Fig. 5** Interaction of aurein 1.2 with DMPC membrane. **a** Change in $\Delta f$ with time on introduction of a 5 μM solution of the peptide into the QCM-D chamber. The response of the third, fifth, seventh and ninth harmonics are shown (*darkest* to *lightest* lines). **b** Corresponding $\Delta f$–$\Delta D$ plot for the 5 μM sample. **c** $\Delta f$–time plot for a 10 μM sample. **d** Corresponding $\Delta f$–$\Delta D$ plot for the 10 μM sample. All $\Delta f$-time plots have been smoothed using the Adjacent-Averaging method, with 20 points of window

An alternative explanation is that aurein 1.2 binds to the surface of membrane, decreasing the interaction between the membrane surface and the bulk solution (Mechler et al. 2007). Thus, the third and fifth harmonics indicate mass loss, because less solution and hence mass is coupled to the membrane, while the seventh and ninth harmonics indicate mass gain, because they only sense the membrane, which has increased in mass due to the addition of the peptide. This suggests that aurein 1.2 associates with the surface of the membrane. Therefore, when combined with the information extracted from Fig. 5c and d, it can be concluded that aurein 1.2 acts via a *carpet mechanism*.

By comparing the $\Delta f$–$\Delta D$ plots for different concentrations, additional information about the mechanism of action of the peptide can be obtained, which is not readily available in either; for example, for aurein 1.2, the high-concentration $\Delta f$–$\Delta D$ plot showed that it disrupted the membrane, and the low-concentration plot showed that it initially binds to the surface. Together, they thus establish that the peptide acts via a surface-based carpet mechanism.

## Case study 4: oncocin

$\Delta f$–$\Delta D$ plots can be used to show more than just the initial addition of peptide to a membrane. Additional experimental steps can also be included in the $\Delta f$–$\Delta D$ plot. In the oncocin case study, we have included the buffer rinse that is performed after peptide addition and incubation (indicated by a star in Fig. 6).

Addition of oncocin to a DMPC membrane reveals a two-stage mechanism (Fig. 6b). The first process [arrow (i) in Fig. 6b] corresponds to a rapid insertion of the peptide into the membrane with no change in dissipation. All harmonics overlap, indicating that there is an even distribution of peptide throughout the membrane (Mechler et al. 2007). Secondly, after this initial interaction, there is a very small and gradual increase in energy dissipation with a small increase in mass [arrow (ii) in Fig. 6b]. This could correspond to either a further addition of peptide behaving in a different manner, and/or a rearrangement of the peptide added during process (i); for example, since it is known that oncocin freely penetrates bacterial membranes (Knappe et al. 2010), the peptide within the membrane may have diffused into the small pockets of trapped solution that exist between the bottom leaflet of the membrane and the quartz chip surface, increasing the energy dissipation.

The buffer rinse, indicated by a star in Fig. 6, removes ca. 50% of the peptide from the membrane. This suggests that insertion is an equilibrium process. Removing peptide from the bulk solution causes peptide within the membrane to diffuse into the solution to compensate. However, this is not completely reversible. In particular, the increase in dissipation observed during process (ii) does not change.

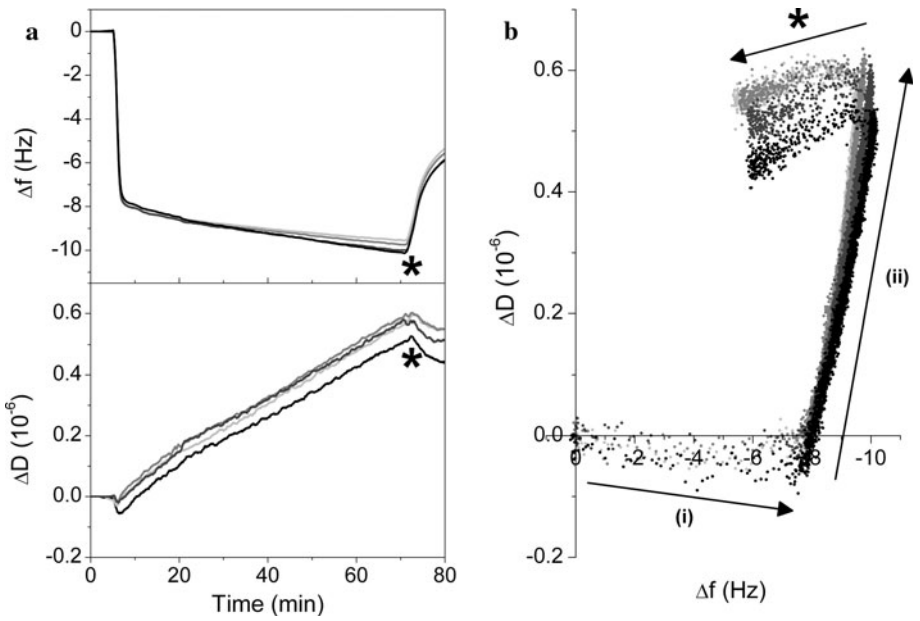


**Fig. 6** Interaction of oncocin with DMPC membrane. **a** Change in $\Delta f$ and $\Delta D$ with time on introduction of a 15 μM solution of the peptide into the QCM-D chamber. At the time point indicated by a *star*, the chamber was flushed with buffer at 300 μl $min^{-1}$. The response of the third, fifth, seventh and ninth harmonics are shown (*darkest* to *lightest* lines). $\Delta f$-time and $\Delta D$-time plots have been smoothed using the Adjacent-Averaging method, with 20 points of window. **b** Corresponding $\Delta f$–$\Delta D$ plot for the 15 μM sample. To assist with interpretation, *arrows* representing each distinct mechanistic process are shown. The *arrows* labelled (i) and (ii) correspond to the first and second processes, respectively, and the *arrow* marked with a *star* corresponds to the buffer rinse

This reinforces the interpretation that either the peptide has bound in a manner that irreversibly changed the membrane structure, or some peptide is trapped at the membrane–chip surface interface.

In conclusion, including the buffer rinse in $\Delta f$–$\Delta D$ plots provides additional information such as the *reversibility* of the peptide interaction, which may assist in understanding its mechanism. In this case study, the non-lytic mechanism of oncocin was established by two observations; firstly, the due-east arrow in the $\Delta f$–$\Delta D$ plot and, secondly, the loss of peptide during the buffer rinse.

## Conclusions

QCM-D can screen potential AMPs for activity towards a variety of membranes and hence determine their selectivity; for example, in case studies 1 and 2 it was concluded that caerin 1.1 wild-type disrupts mammalian membranes, while the mutants do not. Membrane choice is almost limitless, with even complex cell membranes being mimicked in QCM-D [e.g. the stratum corneum membrane of the epidermis (Lee et al. 2009)]. QCM-D can determine the relative potency of the AMP, by determining what concentration of peptide is required for membrane disruption or pore formation. Importantly, QCM-D can investigate the *mechanism of action* of the AMP. Both mass and structural changes to the membrane are detected with time resolution of seconds; for example, the first mechanistic process in case study 2 was over in 15 s. Therefore, QCM-D is a versatile and valuable technique for investigation of AMPs.

The $\Delta f$–$\Delta D$ plot is a useful analytical tool to interpret QCM-D results. This paper has showcased how it can be used to elucidate potential mechanisms for five AMPs with diverse activity. By including all the harmonics in the $\Delta f$–$\Delta D$ plot it is possible to ascertain where the disruption is occurring (a differential response of the harmonics suggests mass loss is occurring at the surface, e.g. case studies 1 and 3), or whether there is aggregation on the membrane (a large energy dissipation at the third harmonic suggests the formation of aggregates, e.g. case study 2). By comparing the $\Delta f$–$\Delta D$ plots for different concentrations, a more complete understanding of the mechanism can be achieved (e.g. case study 3). Finally, including additional steps in the $\Delta f$–$\Delta D$ plot, such as the buffer rinse, gives information about the reversibility of the peptide interaction (e.g. case study 4). Other biophysical techniques can then be used to refine the model.

Furthermore, once the $\Delta f$–$\Delta D$ plot has been used to determine the mechanism of action, it then becomes a *fingerprint* for that peptide. AMPs with similar $\Delta f$–$\Delta D$ plots have similar mechanisms. Therefore, the $\Delta f$–$\Delta D$ plot allows classification of peptides based on their activity towards different membranes. This can lead to a greater understanding of AMPs and, as a result, the development of better antibiotics in the future.

## References


Ambroggio EE, Separovic F, Bowie JH, Fidelio GD, Bagatolli LA (2005) Direct visualization of membrane leakage induced by the antibiotic peptides: maculatin, citropin, and aurein. Biophys J 89:1874–1881

Balla MS, Bowie JH, Separovic F (2004) Solid-state NMR study of antimicrobial peptides from Australian frogs in phospholipid membranes. Eur Biophys J 33:109–116

Briand E, Humblot V, Pradier C-M, Kasemo B, Svedhem S (2010) An OEGylated thiol monolayer for the tethering of liposomes and the study of liposome interactions. Talanta 81:1153–1161

Christ K, Wiedemann I, Bakowsky U, Sahl HG, Bendas G (2007) The role of lipid II in membrane binding of and pore formation by nisin analyzed by two combined biosensor techniques. Biochim Biophys Acta 1768:694–704

Gordon YJ, Romanowski EG, McDermott AM (2005) A review of antimicrobial peptides and their therapeutic potential as anti-infective drugs. Curr Eye Res 30:505–515

Höök F, Kasemo B (2001) Variations in coupled water, viscoelastic properties, and film thickness of a Mefp-1 protein film during adsorption and cross-linking: a quartz crystal microbalance with dissipation monitoring, ellipsometry, and surface plasmon resonance study. Anal Chem 73:5796–5804

IDSA (2004) Bad bugs, no drugs: as antibiotic discovery stagnates, a public health crisis brews. http://www.idsociety.org/. Accessed 28 Sept 2010

Kanazawa KK, Gordon JG (1985) frequency of a quartz microbalance in contact with liquid. Anal Chem 57:1770–1771

Katz ML, Mueller LV, Polyakov M, Weinstock SF (2006) Where have all the antibiotic patents gone? Nat Biotechnol 24:1529–1531

Knappe D, Piantavigna S, Hansen A, Mechler A, Binas A, Nolte O, Martin LL, Hoffmann R (2010) Oncocin (VDKPPYLPRPRPPR-RIYNR-NH2): a novel antibacterial peptide optimized against gram-negative human pathogens. J Med Chem 53:5240–5247

Lam KLH, Ishitsuka Y, Cheng Y, Chien K, Waring AJ, Lehrer RI, Lee KYC (2006) Mechanism of supported membrane disruption by antimicrobial peptide protegrin-1. J Phys Chem B 110: 21282–21286

Lee D, Ashcraft N, Verploegen E, Pashkovski E, Weitz DA (2009) Permeability of model stratum corneum lipid membrane measured using quartz crystal microbalance. Langmuir 25:5762–5766

Marcotte I, Wegener KL, Lam Y-H, Chia BCS, de Planque MRR, Bowie JH, Auger M, Separovic F (2003) Interaction of antimicrobial peptides from Australian amphibians with lipid membranes. Chem Phys Lipids 122:107–120

Mechler A, Praporski S, Atmuri K, Boland M, Separovic F, Martin LL (2007) Specific and selective peptide-membrane interactions revealed using quartz crystal microbalance. Biophys J 93:3907–3916

Mechler A, Praporski S, Piantavigna S, Heaton SM, Hall KN, Aguilar M-I, Martin LL (2009) Structure and homogeneity of pseudo-physiological phospholipid bilayers and their deposition characteristics on carboxylic acid terminated self-assembled monolayers. Biomaterials 30:682–689

Nielsen SB, Otzen DE (2010) Impact of the antimicrobial peptide Novicidin on membrane structure and integrity. J Colloid Interface Sci 345:248–256

Nilebäck E, Westberg F, Deinum J, Svedhem S (2010) Viscoelastic sensing of conformational changes in plasminogen induced upon binding of low molecular weight compounds. Anal Chem 82:8374–8376

Papo N, Shai Y (2003) Exploring peptide membrane interaction using surface plasmon resonance: differentiation between pore formation versus membrane disruption by lytic peptides. Biochemistry 42:458–466

Peschel A, Sahl H-G (2006) The co-evolution of host cationic antimicrobial peptides and microbial resistance. Nat Microbiol 4:529–536

Piantavigna S, Czihal P, Mechler A, Richter M, Hoffmann R, Martin LL (2009) Cell penetrating apidaecin peptide interactions with biomimetic phospholipid membranes. Int J Pept Res Ther 15:139–146

Powers JPS, Hancock REW (2003) The relationship between peptide structure and antibacterial activity. Peptides 24:1681–1691

Pukala TL, Brinkworth CS, Carver JA, Bowie JH (2004) Investigating the importance of the flexible hinge in caerin 1.1: solution structures and activity of two synthetically modified caerin peptides. Biochemistry 43:937–944

Rickert J, Brecht A, Göpel W (1997) QCM operation in liquids: constant sensitivity during formation of extended protein multilayers by affinity. Anal Chem 69:1441–1448

Rodahl M, Kasemo B (1996) On the measurement of thin liquid overlayers with the quartz-crystal microbalance. Sens Actuators A Phys 54:448–456

Rodahl M, Höök F, Krozer A, Brzezinski P, Kasemo B (1995) Quartz crystal microbalance setup for frequency and Q-factor measurements in gaseous and liquid environments. Rev Sci Instrum 66:3924–3930

Rodahl M, Höök F, Fredriksson C, Keller CA, Krozer A, Brzezinski P, Voinova M, Kasemo B (1997) Simultaneous frequency and dissipation factor QCM measurements of biomolecular adsorption and cell adhesion. Faraday Discuss 107:229–246

Rozek T, Wegener KL, Bowie JH, Olver IN, Carver JA, Wallace JC, Tyler MJ (2000) The antibiotic and anticancer active aurein peptides from the Australian bell frogs Litoria aurea and Litoria raniformis. Eur J Biochem 267:5330–5341

Sauerbrey G (1959) The use of quartz oscillators for weighing thin layers and for microweighing. Z Phys 155:206–222

Shai Y (1999) Mechanism of the binding, insertion and destabilization of phospholipid bilayer membranes by K-helical antimicrobial and cell non-selective membrane-lytic peptides. Biochim Biophys Acta 1462:55–70

Shai Y (2002) Mode of action of membrane active antimicrobial peptides. Biopolymers 66:236–248

Sherman PJ, Jackway RJ, Gehman JD, Praporski S, McCubbin GA, Mechler A, Martin LL, Separovic F, Bowie JH (2009) solution structure and membrane interactions of the antimicrobial peptide fallaxidin 4.1a: an NMR and QCM study. Biochemistry 48: 11892–11901

Stone DJM, Bowie JH, Tyler MJ, Wallace JC (1992) The structure of caerin 1.1, a novel antibiotic peptide from Australian tree frogs. J Chem Soc, Chem Commun (17):1224–1225

VanCompernolle SE, Taylor RJ, Oswald-Richter K, Jiang J, Youree BE, Bowie JH, Tyler MJ, Conlon JM, Wade D, Aiken C, Dermody TS, KewalRamani VN, Rollins-Smith LA, Unutmaz D (2005) Antimicrobial peptides from amphibian skin potently inhibit human immunodeficiency virus infection and transfer of virus from dendritic cells to T cells. J Virol 79:11598–11606

Voinova MV, Rodahl M, Jonson M, Kasemo B (1999) Viscoelastic acoustic response of layered polymer films at fluid-solid interfaces: continuum mechanics approach. Phys Scr 59:391–396

Wong H, Bowie JH, Carver JA (1997) The solution structure and activity of caerin 1.1, an antimicrobial peptide from the Australian green tree frog, Litoria splendida. Eur J Biochem 247:545–557

Zasloff M (2002) Antimicrobial peptides of multicellular organisms. Nature 415:389–395